Fuel 428 (2027) 140456

Contents lists available at ScienceDirect

Fuel

journal homepage: www.elsevier.com/locate/jfue

Full Length Article

CFD modelling of methanol RCCI combustion in low load marine engine conditions - A comparative study with conventional dual-fuel combustion

Konstantinos Zoumpourlos [a,*], Cemil Bekdemir [b], Konstantinos Ioannis Kiouranakis [a], Rinze Geertsma [c], Robert van de Ketterij [c], Andrea Coraddu [a]

[a] Delft University of Technology, Delft, the Netherlands
[b] TNO Powertrains, Helmond, the Netherlands
[c] Netherlands Defence Academy, Den Helder, the Netherlands

HIGHLIGHTS

- Full marine engine CFD model of methanol RCCI and CDF combustion at low load.
- Methanol reactivity stratification governs ignition kernels and heat-release shaping.
- Lower RCCI combustion temperatures result in significantly reduced NOx emissions.
- Lean methanol-air pockets lead to high THC and reduced combustion efficiency.

ARTICLE INFO

Keywords:
Methanol
Internal combustion engines
Computational fluid dynamics
Dual-fuel engine
Port fuel injection
Alternative fuels

ABSTRACT

Methanol reactivity controlled compression ignition (RCCI) is considered a promising combustion strategy for future low-carbon marine engines, due to its potential for low NOx emissions and high indicated thermal efficiency. This study presents three-dimensional CFD simulations of methanol–diesel RCCI in a single-cylinder maritime engine at low load. The model employs SAGE detailed chemistry using a methanol/n-heptane skeletal mechanism and validated spray sub-models. To analyse the impact of earlier diesel injection timing, we compared two RCCI simulation cases, with 58% and 64% methanol blending ratios (BRs), against a conventional dual-fuel (CDF) case. Our simulation results show good agreement with measured in-cylinder pressure and apparent heat release rate (AHRR), accurately capturing ignition timing, overall combustion phasing, and measured NOx emissions. By conducting an in-cylinder analysis, we reveal that methanol premixing induces reactivity stratification through its combustion inhibitory effect. This reactivity stratification determines the ignition kernels, while the RCCI operating strategy, combining earlier diesel injection with different methanol blending and intake-temperature conditions, produces a more distributed ignition area. Thus, under the investigated low-load conditions, RCCI exhibits lower peak temperatures and thereby decreased NOx emissions, while maintaining comparable gross indicated thermal efficiency to CDF. However, at very lean methanol conditions, incomplete oxidation in the near-wall cylinder liner region increases unburned hydrocarbon (THC) emissions and hinders combustion efficiency. Our findings highlight the importance of mixture stratification in methanol RCCI and provide guidelines for the improvement of future methanol-fuelled marine and heavy-duty engines.

1. Introduction

Reciprocating internal combustion engines (ICEs) will continue to dominate marine power systems in the foreseeable future, making their decarbonization a priority [1–5]. Renewable methanol is among the most mature and scalable alternative marine fuels [6–9], offering significant reductions in greenhouse-gas emissions, particulate matter (PM) and NOx emissions compared to diesel compression ignition (CI) engines [10]. Methanol's main limitation to its adoption in marine engine applications is its high autoignition temperature, which makes conventional mixing-controlled CI combustion very challenging [11]. While

* Corresponding Author.
Email addresses: k.zoumpourlos@tudelft.nl; kon.zoumpourlos@gmail.com (K. Zoumpourlos), cemil.bekdemir@tno.nl (C. Bekdemir), k.i.kiouranakis@tudelft.nl (K.I. Kiouranakis), rd.geertsma@mindef.nl (R. Geertsma), a.coraddu@tudelft.nl (A. Coraddu).

https://doi.org/10.1016/j.fuel.2026.140456
Received 7 April 2026; Received in revised form 16 June 2026; Accepted 21 June 2026
Available online 30 June 2026

Nomenclature

CO	Carbon Monoxide
NOx	Nitrogen Oxides
AHRR	Apparent Heat Release Rate
BR	Blending Ratio
CAD	Crank Angle Degree
CDF	Conventional Dual-Fuel
DF	Dual-Fuel
DI	Direct Injection
HD	Heavy-Duty
HRF	High Reactivity Fuel
ICE	Internal Combustion Engine
LRF	Low Reactivity Fuel
LTC	Low-Temperature Combustion
PFI	Port Fuel Injection
RCCI	Reactivity-Controlled Compression Ignition
TDC	Top Dead Center
THC	Unburned Hydrocarbons

spark ignition (SI) is possible and more fitting for methanol fuel, knock constraints limit compression ratio and power density, rendering it unsuitable for high efficiency heavy-duty and marine engines Mahendar et al. [12].

Dual-fuel CI strategies overcome this limitation by using a small diesel pilot to ignite methanol [13]. In large low-speed two-stroke and medium-speed four-stroke engines, mixing-controlled (diffusion) combustion is the most practical approach for high-methanol blending ratio (BR) robust operation, with both fuels being directly injected at high pressure [14]. However, for high-speed four-stroke marine engines, port fuel injection (PFI) of methanol combined with diesel direct injection (DI) is more feasible due to cylinder-head size constraints [15]. This premixed configuration yields stronger NOx and PM reductions than diffusion-based DF combustion systems [16].

Within this PFI/DI framework, two premixed regimes are possible. Conventional dual-fuel (CDF) combustion uses the diesel pilot as a 'liquid spark', which, upon its autoignition, generates multiple ignition kernels that form several flame fronts propagating through the methanol-air mixture. This multi-flame structure allows flames to traverse the large combustion chambers of marine engines sufficiently fast to avoid knock, an issue that would be challenging with bulk turbulent flames typical of SI operation at the lean mixture levels in diesel engines [17,18]. CDF can achieve high efficiencies, low NOx and high BRs at medium-to-high loads [19,20]. However, at low loads, the unthrottled operation of diesel engines produces highly lean mixtures that undermine flame propagation and combustion performance, resulting in lower fuel economy and high unburned hydrocarbon (THC) emissions [21,22].

These limitations motivate the second premixed regime: reactivity controlled compression ignition (RCCI), which evolved from the homogeneous charge compression ignition (HCCI) concept [23–28]. Unlike the flame-propagation-dominated combustion physics of CDF, HCCI/RCCI targets a well-mixed fuel–air charge prior to ignition, with combustion governed primarily by distributed autoignition [29–31]. Similar to HCCI, RCCI seeks to combine the benefits of SI-like premixed combustion (low soot) with those of CI-like lean operation (high efficiency), while overcoming the typical control challenges of HCCI [32,33]. The central limitation of single-fuel HCCI is that a fixed fuel reactivity forces trade-offs across the engine load range: high reactivity (low octane/high cetane) favours low-load stability, whereas low reactivity (high octane/low cetane) is preferable at higher loads to avoid knock [34–39]. Rather than selecting a fuel with an 'average' compromise, RCCI leverages two fuels of opposing reactivity [40]. Here, a tailored ratio and stratification between a low-reactivity fuel (LRF), such as methanol and a high-reactivity fuel (HRF), such as diesel, can achieve optimal performance across the entire engine load envelope. RCCI can enable stable lean-burn operation at air-fuel ratios well beyond CDF's flammability limits while retaining unthrottled operation. The resulting nearly volumetric heat release delivers efficiencies that exceed those of conventional diesel engines, while simultaneously achieving low NOx and near-zero soot. Therefore, a complementary strategy of RCCI at low loads and CDF at medium-to-high loads, mirroring established mode concepts in gasoline HCCI-SI and diesel-DICI systems, can enable high-efficiency across the engine operating envelope [41–44].

Despite methanol's beneficial charge-cooling and high-octane characteristics that favour low NOx and high efficiency, these properties, together with methanol's inhibition of diesel's low-temperature heat release, limit the maximum diesel replacement that can be achieved in practice [45–47]. For example, Zou et al. [48] reported that at part load, methanol needed to be limited to the greatest extent compared to ethanol, n-butanol, and gasoline when used as the LRF in RCCI to preserve combustion stability. Advancing understanding of these mechanisms under realistic engine conditions, specifically, the spatial distribution of the methanol-air charge, the resulting reactivity gradients, and their coupling to ignition and heat-release dynamics, is therefore crucial to improve the controllability and robustness of methanol RCCI. However, methanol-specific RCCI studies remain scarce, both experimentally and numerically. Most numerical studies ignore the PFI-driven in-cylinder methanol stratification by assuming a homogeneous methanol-air mixture. This is critical to reactivity gradients, the interactions with the diesel, the onset of ignition and subsequent heat release evolution, and ultimately, the overall efficiency and emissions. This leaves a critical gap in the physical understanding required to advance the concept beyond its current operational boundaries and support its broader commercial adoption in marine ICEs.

1.1. AIM and novelty

Although methanol has received attention as a premixed fuel in marine dual-fuel engines, methanol RCCI studies remain limited, especially those using full engine-geometry CFD models. Previous numerical investigations imposed a perfectly premixed methanol–air charge in the combustion chamber, which enables simplified axisymmetric or sector-based simulations while avoiding the complexity of realistic in-cylinder mixture preparation [48–51]. As a result, studies focusing on larger-bore marine dual-fuel engines remain scarce, especially at high methanol fractions, where RCCI strategies become highly sensitive to local mixture stratification. The majority of methanol dual-fuel simulations use low methanol injection pressures (3–10 bar), which limit evaporation rates and hinder air-fuel mixing.

To address the presented literature gaps, we investigate low load methanol RCCI combustion and compare it with the late-injection CDF approach. In contrast to previous low pressure PFI literature, our work employed a high-pressure methanol injection system aimed at improving mixture formation and achieving elevated methanol BRs. To validate our models, we utilised experimental data from a 4-L dual-PFI single-cylinder high-speed marine engine operating under both CDF and RCCI. The novelty of our approach lies in a full-cylinder 3D engine model that integrates state-of-the-art spray modelling, methanol–air mixture formation, and combustion governed by detailed chemical kinetics. The framework was implemented in CONVERGE-CFD and incorporates the authors' methanol spray modelling framework, which was extensively validated using methanol and diesel experimental datasets [52–54].

Additionally, the RCCI model was developed based on our recently developed CDF combustion model Bùi et al. [55]. By not assuming a homogeneous methanol mixture, this study accounts for the spatially varying in-cylinder fuel–air distribution, which influences ignition, reactivity gradients, and combustion phasing in methanol RCCI operation. Consequently, our results provide new insights into the combustion behaviour of contemporary methanol–diesel marine engines and support the development of future low-carbon, high-efficiency propulsion systems.

2. Measurement setup - single cylinder marine engine

The CFD framework has been validated against measurements from the marine single-cylinder research engine described in detail by Kiouranakis et al. [56]. The engine features a bore and stroke of 170 mm and 180 mm, respectively, and a compression ratio of 14:1; its main specifications are listed in Table 1. In-cylinder pressure was acquired at 0.1°CA resolution using a piezoelectric transducer over 50 consecutive cycles. The raw pressure traces were filtered with a first-order Savitzky-Golay filter, and the ensemble-averaged pressure was used as input for AHRR calculations.

Table 2 illustrates the simulated operating conditions, which correspond to each of the experimental CDF and RCCI cases. The conditions correspond to experimentally realised operating points rather than an idealised parametric sweep. Consequently, BR and intake temperature differ among the cases because they reflect the stable operating conditions achieved in the test engine for each combustion mode. Keeping BR and intake temperature identical across CDF and RCCI would improve direct numerical comparison, but would no longer correspond to the available validation measurements. Therefore, the CDF–RCCI comparison should be interpreted as a comparison between experimentally demonstrated operating strategies, while the RCCI-1/RCCI-2 comparison indicates the combined influence of BR, methanol lambda, and intake temperature within RCCI operation. For each case, the BR is calculated based on the methanol energy fraction, as in our previous study [55]. The BR is defined on the energy basis as shown in Eq. (1).

$$BR = \frac{\dot{m}_{CH3OH} \cdot LHV_{CH3OH}}{\dot{m}_{CH3OH} \cdot LHV_{CH3OH} + \dot{m}_{diesel} \cdot LHV_{diesel}} \cdot 100\%, \quad (1)$$

Table 1
Test engine specifications.

Items	Specification
Number of cylinder	1
Bore (mm)	170
Stroke (mm)	180
Displacement (L)	4
Compression ratio	14:1
Speed (rpm)	1500
Number of nozzles per methanol injector	6
Methanol nozzle diameter (mm)	0.197
Methanol injection pressure (bar)	100–140
Number of nozzles per diesel injector	10
Diesel nozzle diameter (mm)	0.270
Diesel injection pressure (bar)	310–360

Table 2
Baseline operating conditions for conventional DF and RCCI cases at 3.1 bar BMEP.

Parameters	CDF	RCCI-1	RCCI-2
$\dot{m}_{inj,diesel}$ [kg/h]	2.13	1.80	1.57
$\dot{m}_{inj,methanol}$ [kg/h]	5.47	5.42	5.86
Diesel SOI [°]	−14.4	−39.4	−39.4
BR [%]	55	58	64
λ_{MeOH}	6.6	7.4	6.8
T_{intake} [K]	353.1	305	318
P_{intake} [kPa]	120	120	120
$T_{exhaust}$ [K]	570.1	538	543
$P_{exhaust}$ [kPa]	124.5	120	120

where $\dot{m}$ and LHV denote the mass flow rate and lower heating value of each fuel, respectively.

3. Computational method

In this section, we introduce the CFD modelling approach, developed in CONVERGE v3.1 [57]. Since the present study is a continuation of our earlier spray [52–54] and marine engine combustion [55] modelling, we refer to them for further details on the underlying sub-models. Fig. 1 shows the computational domain used to represent the single cylinder experimental setup. A methanol injector was installed at each intake runner, with the fuel spray direction targeting the cylinder along the air path. To accommodate the pilot diesel injection, a ten-hole diesel injector was located at the centre of the cylinder head.

For the grid generation, we employed the CONVERGE cut-cell Cartesian method [58,59] using a base cell size of 8 mm. To capture spray and combustion phenomena, adaptive mesh refinement (AMR) was applied based on velocity and temperature gradients, achieving a minimum cell size of 0.250 mm. AMR was also used during the intake and exhaust strokes, obtaining 1 mm cells in the respective cylinder and intake and exhaust manifold regions. The sub-grid embedding criterion for the AMR was set as 1 m/s for the velocity and 2.5 K for the temperature refinement. Furthermore, we pre-refined certain regions of interest using fixed embedding. Particularly, a cell size of 2 mm was assigned near the piston crown, the cylinder head, and along the liner throughout the cycle; 0.5 mm cells were used in the valve seat region during valve motion. For each injector, the mesh was refined within a conical region to 0.5 mm during the injection event. Lastly, a small cylindrical embedding was also included at each nozzle outlet to better capture air entrainment and early spray development. We ensured that our mesh sizing complies with other CFD spray and combustion studies [60–62] and provides credible results. The maximum number of computational cells reached approximately 6.5 million during combustion.

Several sub-models were incorporated to capture turbulence, multiphase flow, and combustion. Turbulence was resolved using the RNG k–ϵ model [63]. Multiphase flow was treated with the discrete phase model [64], which uses parcels in a Lagrangian framework, while the gaseous phase is solved using the Eulerian formulation. Regarding the Lagrangian parcels, we employed the blob injection model [65], while the primary and secondary breakup were estimated by the KH-RT model [66]. Droplet interactions were captured using the No-Time-Counter (NTC) method [67] coupled with the Post-Collision

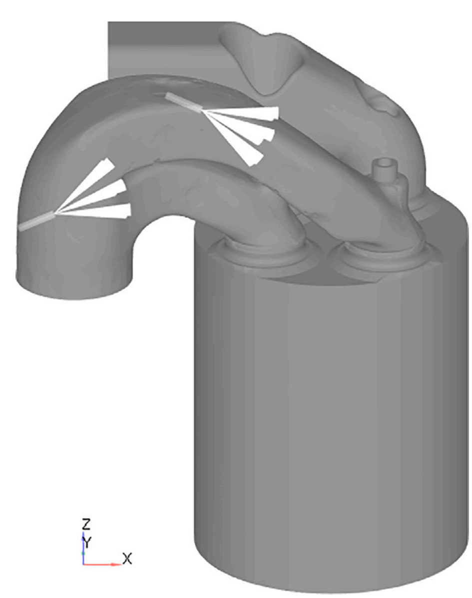

Fig. 1. Single cylinder computational domain.

Table 3
Spray and Combustion Sub-models.

Physical Phenomena	Numerical models
Droplet injection	Blob model [65]
Droplet breakup	KH-RT model [66]
Droplet collision	No Time Counter model [67]
Droplet coalescence	Post Collision Outcome model [68]
Spray/wall interaction	Kuhnke model [69]
Droplet evaporation	Frossling model [64]
Liquid film evaporation	Film Evaporation model [64]
Combustion model	SAGE Detailed Chemistry [72]
Chemical mechanism	Liu et al. [70] (52 species, 182 reactions)
NOx formation	Extended Zel'dovich mechanism [58]

Outcome model [68], while spray wall interaction was modelled by the Kuhnke film splash model [69]. Additionally, droplet evaporation was computed using the Frössling correlation, and liquid-film vaporization utilised the wall-film model of Richards et al. [64]. These modelling choices were consistent with the authors' prior methanol spray work under marine-engine conditions [53,54].

Similarly to Bùi et al. [55], for combustion modelling, the SAGE detailed chemical-kinetics solver [64] was used along with the reduced mechanism of Liu et al. [70]. To simplify the chemistry calculations, a single-component diesel surrogate, n-heptane ($nC7H16$), was used to obtain reliable ignition-delay predictions for the dual-fuel simulations [71]. Diesel liquid properties were assigned to the Lagrangian parcels, while n-heptane was used for the gaseous phase. Finally, the extended Zel'dovich mechanism was used to model NOx formation [58]. An overview of all spray and combustion sub-models is provided in Table 3.

4. Results and discussion

In this section, we present the validation and analysis of the developed CFD framework for the simulated methanol–diesel cases. It should be noted that the validation is limited to the available low-load experimental operating points at 3.1 bar BMEP and 1500 rpm. Therefore, the present model should be interpreted as validated for the investigated operating window rather than as a fully general predictive tool across the entire engine map. Additional validation at higher loads, different speeds, and broader methanol blending ratios is required before generalising the conclusions to other marine-engine operating conditions.

Initially, we compare the predicted in-cylinder pressure and apparent heat release rate (AHRR) with experimental data for both the baseline CDF and the RCCI cases. In addition to pressure and AHRR, NOx predictions are compared against available experimental measurements in Section 4.3. Experimental THC and CO data were not available for the present dataset; therefore, the THC and CO results are interpreted as model-based trends rather than fully validated absolute predictions. We then extend the analysis using in-cylinder spatial fields during ignition and flame propagation. These fields illustrate how the RCCI operating conditions, including earlier diesel injection, altered methanol blending ratio, and different intake temperature, modify methanol ignition behaviour and subsequent flame development. Because BR and intake temperature differ between the CDF and RCCI cases, the present comparison cannot isolate the independent effect of diesel SOI. A dedicated parametric study with fixed BR and intake temperature would be required to quantify the isolated SOI effect. Consequently, performance and emissions trends are analysed, including the impact of early diesel injection on efficiency, NOx, CO, and THC formation. Finally, the role of methanol mixture stratification is compared with a perfectly homogeneous case, highlighting its influence on both ignition and subsequent combustion behaviour.

4.1. Model validation

Fig. 2 compares the simulated in-cylinder pressure and AHRR against experimental data for the baseline CDF and the two RCCI cases. Overall, the CFD model results agree adequately with the experimental data,

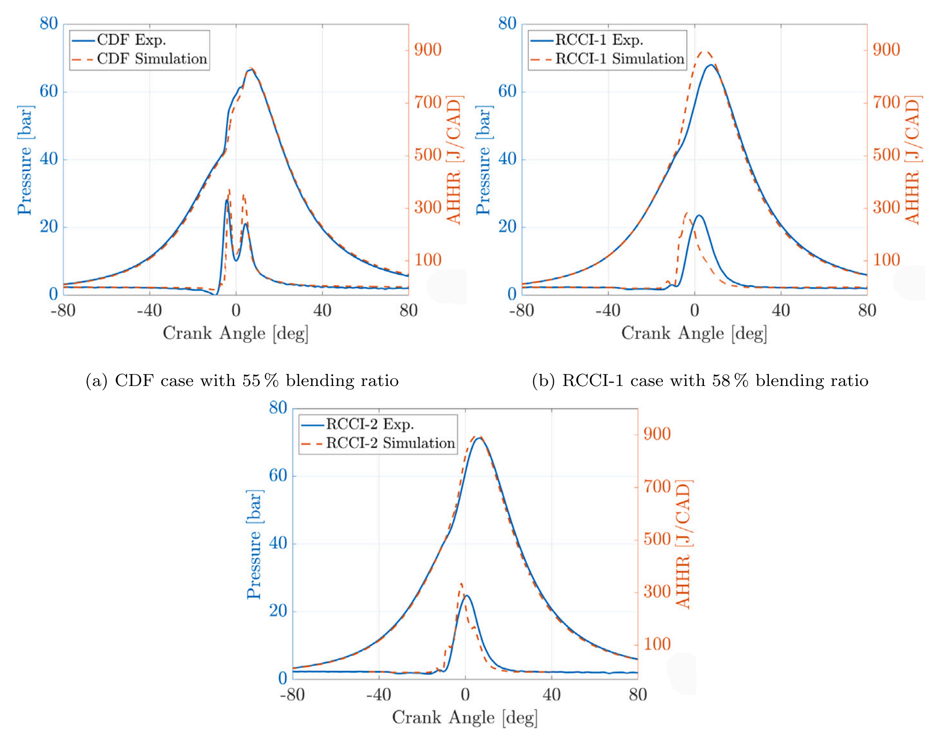

(a) CDF case with 55 % blending ratio

(b) RCCI-1 case with 58 % blending ratio

(c) RCCI-2 case with 64 % blending ratio

Fig. 2. Comparison between numerical and experimental in-cylinder pressure and AHRR for the investigated CDF and RCCI cases.

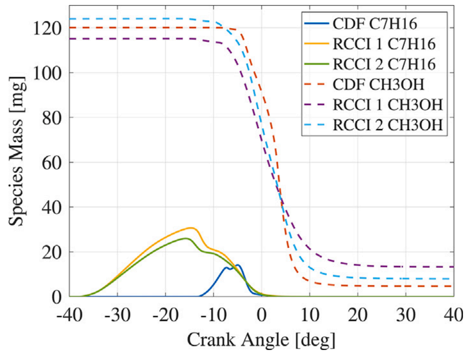

Fig. 3. Mass of both fuels in the cylinder around TDC.

particularly for the CDF (Fig. 2a) and RCCI-2 (Fig. 2c) cases. With respect to the AHRR trends, the CFD model successfully reproduced the distinct shapes for each simulation case: specifically, the two-peak AHRR representing two combustion stages in the CDF, and the single-peak bell-like shape in the RCCI cases. Moreover, the ignition timing is captured satisfactorily, while both the overall burn duration and peak pressure are predicted accurately within 1% error.

For the RCCI-1 case, however, the ignition delay is under-predicted, resulting in an earlier start of combustion and a corresponding over-prediction of the peak cylinder pressure. This discrepancy can be attributed to the fact that the CFD framework was primarily tuned for the higher BR conditions of RCCI-2, and subsequently applied to RCCI-1 with only minimal adjustments. These adjustments mainly involved applying the appropriate boundary conditions, while the spray and combustion model settings were kept the same as in the CDF and RCCI-2 cases. The previously mentioned tuning concerns the diesel injection settings, which significantly influence HRF-air mixing, such as the injection cone angle, the mass-flow rate shape, and the nozzle discharge and velocity coefficients. The inherent discrepancy in RCCI-1 indicates that the model is less accurate for the leaner RCCI condition. Nevertheless, the RCCI-1 under-prediction of ignition delay suggests that quantitative conclusions for this case, particularly peak pressure and combustion phasing, should be interpreted with caution. Despite this, the RCCI-1 peak pressure shows an error of approximately 5%, which is deemed acceptable for the qualitative analysis in the remainder of the paper.

Fig. 3 presents the in-cylinder masses of methanol and n-heptane around TDC. Both RCCI cases show slower methanol consumption than the baseline CDF case. This behaviour reflects the combined effects of increased methanol λ and advanced n-heptane injection on ignition and flame propagation. Moreover, in the RCCI cases, the even slower consumption of n-heptane highlights the slower kinetics-driven autoignition characteristic of LTC combustion. After combustion, the residual methanol shows a relatively high level of unburned fuel, consistent with

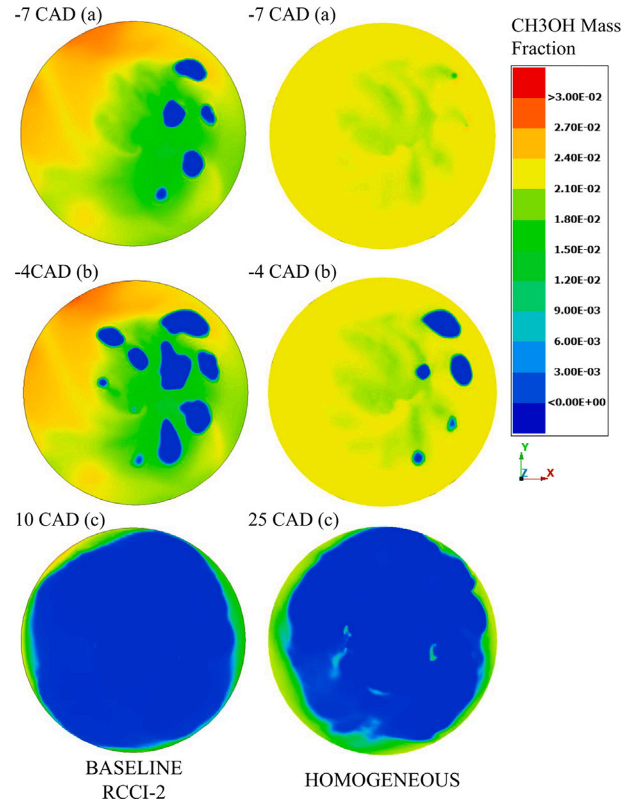

Fig. 5. Methanol mass fractions during ignition (a), during combustion (around CA10) (b), and at the end of combustion (after CA90) (c) of homogeneous and baseline inhomogeneous cases for the RCCI-2 condition at $z = -1.5$ mm XY-plane.

our previous study [55]. The RCCI cases, however, exhibit much higher levels of unburned methanol, an outcome examined in more detail in the following sections.

4.2. In-cylinder combustion characteristics

4.2.1. Influence of mixture homogeneity

Since mixture stratification plays a decisive role in determining autoignition behaviour in RCCI combustion, one should evaluate the extent to which reactivity stratification influences the simulated engine. Much of the existing numerical literature assumes a perfectly homogeneous fuel–air mixture, which greatly simplifies the problem but may not reflect the actual conditions in methanol PFI engines. In this section, we evaluate the validity of the homogeneous-mixture assumption by comparing the RCCI-2 case with an ideal condition in which methanol is

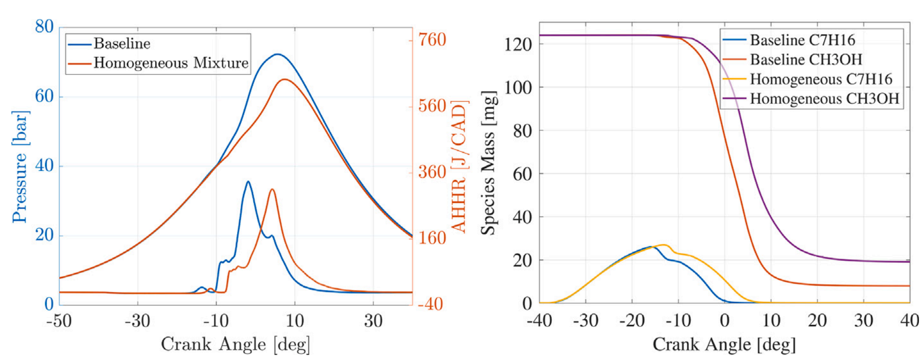

Fig. 4. Pressure (a), AHRR (a), and fuel mass consumption comparisons of homogeneous and baseline inhomogeneous cases for the RCCI-2 condition.

well mixed. The homogeneous-mixture comparison was performed only for RCCI-2 because this case combines the highest methanol blending ratio with the best agreement against the available experimental pressure/AHRR data. Therefore, the comparison is intended to demonstrate the physical importance of methanol stratification for the representative high-BR RCCI case, rather than to provide a complete parametric assessment across all RCCI conditions.

The homogeneous RCCI-2 case was initialised using the same total methanol and n-heptane masses as the baseline RCCI-2 case. Methanol was uniformly distributed in the cylinder at IVC (at 150 CAD), while the same diesel injection timing, injection mass, boundary conditions, and combustion sub-model settings were retained. Therefore, the comparison isolates the influence of methanol spatial distribution while keeping the total fuel energy input constant. Fig. 4 demonstrates that assuming a perfectly homogeneous methanol mixture fundamentally alters the RCCI combustion characteristics. In the homogeneous case, the absence of reactivity stratification suppresses the high-reactivity gradients that govern ignition. Subsequently, the suppression of the ignition kernels delays and weakens autoignition, lowering the peak in-cylinder pressure and altering the shape of the AHRR compared with the stratified case (Fig. 4a). Likewise, in Fig. 4(b), the fuel-consumption trends show that the homogeneous simulation slows both methanol and heptane oxidation. This confirms the hypothesis that fuel stratification, established through methanol PFI simulation, is crucial for accurately predicting combustion phenomena.

Furthermore, Fig. 5 illustrates the methanol mass fraction contour plots. Due to the inherent differences in combustion, we depict different crank angle snapshots for each case reflecting similar combustion phases between the simulation cases. The figure shows that the homogeneous case lacks the local methanol-lean pockets, which normally act as high-reactivity regions and promote heptane ignition. Thus, in the homogeneous case, combustion initiates in the high-concentration heptane

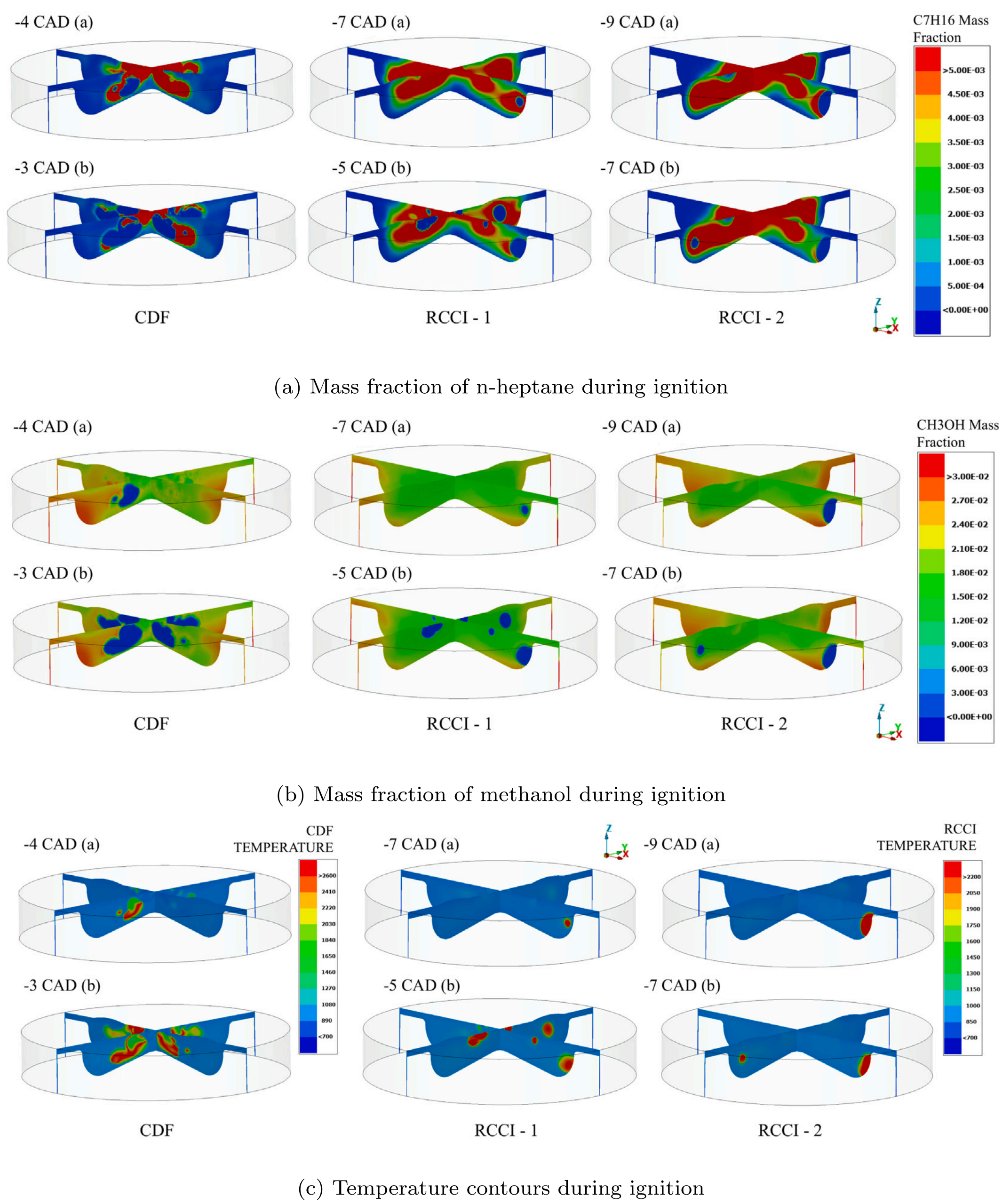

(a) Mass fraction of n-heptane during ignition

(b) Mass fraction of methanol during ignition

(c) Temperature contours during ignition

Fig. 6. Fuel mass fractions and temperature contours during ignition.

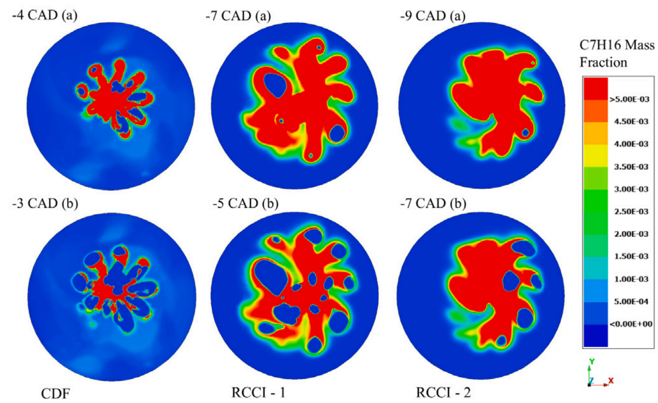

(a) Mass fraction of n-heptane during ignition. In the CDF case, as n-heptane is injected and combusting earlier, the snapshots are depicting earlier crank angles for visualisation purposes.

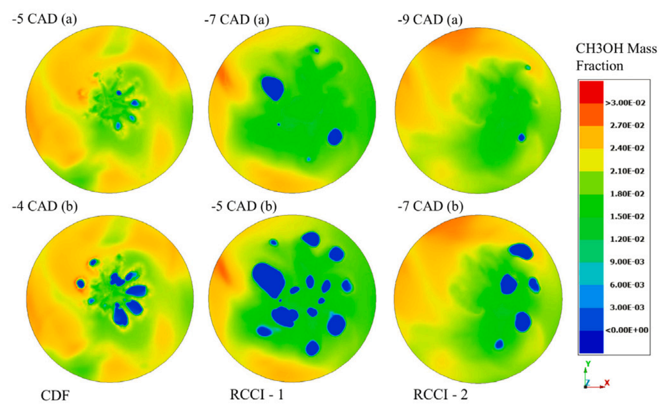

(b) Mass fraction of methanol during ignition

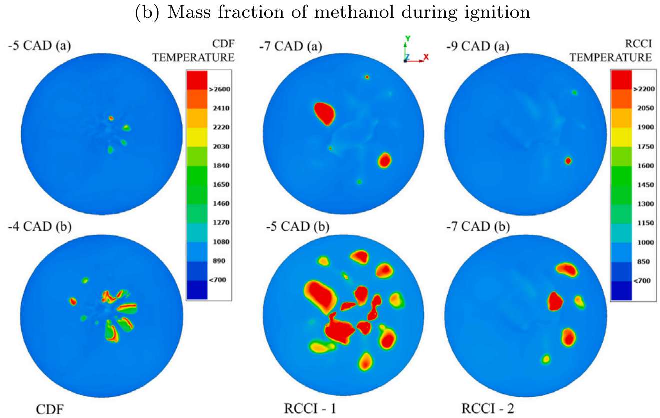

(c) Temperature contours during ignition

Fig. 7. Fuel mass fractions and temperature contours at z = − 1.5 mm XY-plane during ignition.

regions, which serve as the main high-reactivity zones. Although these ignition locations are similar to those in the stratified case, the increased ambient methanol concentration inhibits the reactions and increases the ignition delay. As the homogeneous case exhibits a longer ignition delay, the later stages of combustion (Fig. 5c) are presented much later compared to the baseline stratified case (at 25 CAD instead of 10 CAD). The delayed combustion development results in lower methanol burn-rates and, eventually, increased unburned methanol quantities near the cylinder liner. In contrast, the stratified case exhibits regions of reduced methanol concentration, which promote earlier autoignition and faster flame propagation.

The stratified case should not be interpreted as universally superior. Stratification promotes earlier ignition and faster methanol consumption, which benefits combustion phasing and gross ITE. However, excessive or poorly controlled stratification may also create locally over-lean, over-rich, or near-wall regions that increase incomplete oxidation as well as THC and CO emissions. Therefore, the objective is not complete homogeneity or maximum stratification, but controlled reactivity stratification. These findings highlight the importance of explicitly modelling mixture stratification in obtaining more realistic methanol-diesel combustion predictions in PFI engines. Such CFD studies could be used to further optimise the geometry of both the combustion chamber and the inlet ports, along with their effect on cylinder swirl and tumble to improve combustion.

4.2.2. The role of methanol stratification in diesel ignition

In this section, we qualitatively assess the reactivity stratification for each simulation case. The spatial distributions of heptane and methanol mass fractions, together with the corresponding temperature fields, are examined following common practice in RCCI analyses [73,74]. The present interpretation of reactivity stratification and near-wall incomplete oxidation is based primarily on qualitative analysis of the resolved CFD fields. Fig. 6(a) and Fig. 6(b) illustrate the heptane and methanol mass fractions for all cases. Using perpendicular ZY and ZX cut-planes during the ignition phase of each case, we demonstrate the locations of the initial ignition kernels within the heptane–methanol–air mixture. Heptane, as the high-reactivity fuel, ignites first and establishes the reaction zones, which then consume methanol and initiate premixed flame propagation into the methanol–air mixture. Fig. 6(c) depicts the corresponding temperature fields during ignition. For the CDF case, the temperature scale is shifted by 400 K to account for the higher temperatures associated with mixing-controlled heptane combustion. This temperature scale offset is a graphical post-processing choice used only for visualisation purposes.

In Fig. 7, the same sequence of snapshots is shown from a different perspective, using a cut-plane perpendicular to the cylinder axis at an offset distance of 1.5 mm from the cylinder head. In the CDF case, the heptane spray plumes are clearly visible along with the corresponding ignition spots that form along these plumes. On the contrary, the RCCI cases exhibit ignition initiation in regions where the methanol concentration is lower than average. Due to methanol's reaction inhibition effect [75], these locally methanol-lean zones possess higher reactivity and thus serve as the initial ignition kernels. The kernels then grow along the paths of lower methanol concentration, consistent with the imposed reactivity stratification. Specifically, the HRF governs ignition onset and establishes the reaction zones, while the LRF contributes to the subsequent heat release as temperatures rise. Moreover, in the RCCI cases, the early-stage temperature rise is decreased and more distributed compared to CDF, reflecting low-temperature chemistry prior to the main heat release, as shown in Fig. 2. When high methanol fractions overlap with low-temperature regions, methanol's high latent heat and lower reactivity hinder ignition, relative to the CDF case, contributing to smoother AHRR and reduced peak temperatures that influence NOx formation.

Figs. 8 and 9 illustrate the computational cell-based lambda-temperature distributions for the CDF and RCCI cases before ignition and during the main combustion phase. In the CDF case, before ignition, the late injection of heptane produces a wide spread of lambdas, spanning both fuel-rich and lean conditions. This is typical of mixing-controlled combustion and promotes the formation of localised high-temperature zones once ignition occurs. During combustion, the majority of the CDF case cells exhibit much greater temperatures than those in the RCCI cases, with lambdas clustered closer to stoichiometry.

In contrast, the RCCI cases differ in the heptane lambda distribution due to earlier injection timing, which enables premixing with the surrounding methanol–air charge. As a result, in Fig. 8, the lambda

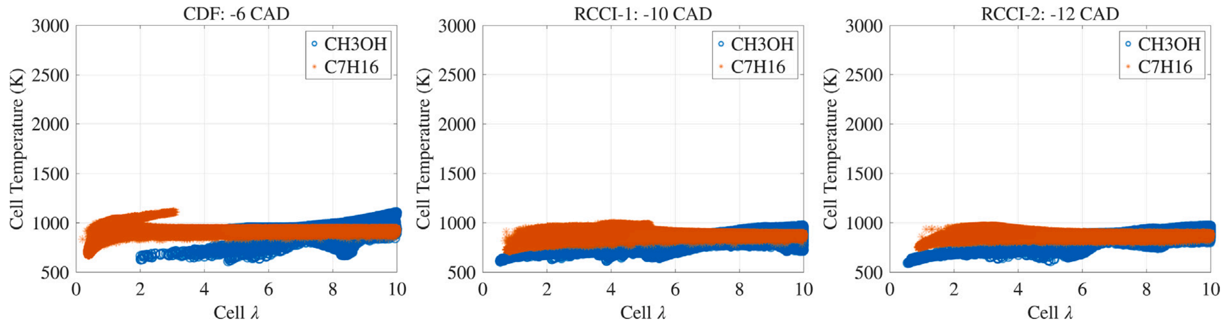

Fig. 8. Cell lambda and temperature scatter plot for the simulated cases before ignition.

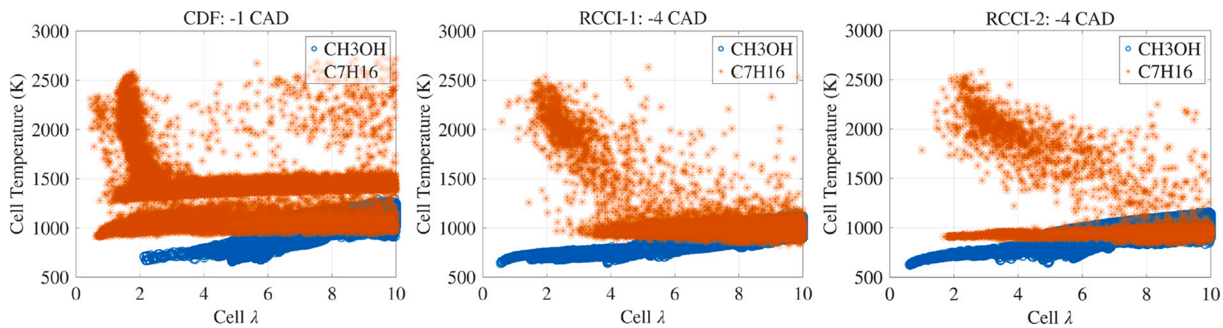

Fig. 9. Cell lambda and temperature scatter plot for the simulated cases during combustion (corresponding approximately to CA10 for each case).

distributions are widespread on the lean side (lambdas higher than unity), while substantially fewer cells occupy richer mixtures. This lean-premixed condition facilitates low-temperature diesel combustion, thereby greatly reducing NOx emissions. During combustion, in Fig. 9, the RCCI scatter plots retain their cell clustering on the lean side, confirming that the premixed charge, combined with methanol's inhibitory effect, sustains lower combustion temperatures.

4.2.3. Flame propagation

In this section, we present the in-cylinder analysis of the combustion phenomena that follow the onset of autoignition. Similarly to the previous section, we use perpendicular ZY and ZX cut-planes (Fig. 10) and XY-plane slices at 1.5 mm distance from the cylinder head (Fig. 11) to illustrate the evolution of the main combustion phase for each simulation case. In Fig. 10(a) and Fig. 11(a), the methanol mass fraction fields suggest a rapid consumption of methanol, driven by fast flame propagation within the premixed methanol–air mixture. The flame front develops considerably faster in the RCCI cases than in the CDF case, due to a larger initial autoignition region resulting from the more uniformly distributed heptane. This behaviour is consistent with the earlier ignition kernels observed in the RCCI cases and explains the broader and more uniform progression of the main combustion event. Furthermore, in the RCCI cases, methanol is progressively consumed from the HRF-initiated reaction zones outward into the bulk air-fuel charge, leading to a smoother heat-release process. On the contrary, in the CDF case, there is a brief period after ignition during which flame propagation has not yet developed. After 4 CAD, the second stage of heat release commences (corresponding to the second peak in the AHRR curve in Fig. 2a), where the rapid flame-propagation phase consumes the remainder of the premixed methanol–air charge. In all simulation cases, flame quenching occurs near the cold cylinder-liner wall, which may become one of the primary sources of unburned methanol emissions.

In the RCCI cases, temperature contours during the ignition period show the formation of multiple ignition kernels that coalesce into larger reaction zones, as shown in Fig. 6(c), Fig. 7(c), Fig. 10(b), and Fig. 11(b). These kernels expand over time and form more evenly distributed high-temperature zones, reaching approximately 2200 K, which in turn initiate the rapid flame propagation in the methanol-air charge. This even distribution of high temperatures is consistent with the bell-like RCCI AHRR shape, differentiating it from CDF combustion. In the CDF case, the mixing-controlled ignition creates localised hot-spots around the spray-plume periphery, which are characteristic of diffusion-dominated combustion. As heptane burns under comparatively richer conditions (Fig. 9), the resulting auto-ignition temperatures are significantly higher than those observed in the RCCI cases, contributing to elevated NOx emissions. As a result, CDF exhibits more localised HRF-dominated autoignition with steep temperature gradients, whereas RCCI distributes the early-stage reactions over a broader area governed by methanol reactivity stratification. Across all cases, consumption of the premixed methanol occurs at relatively low temperatures, around 1100 to 1200 K, as shown by the light-green contours.

4.3. Efficiencies and emissions

Fig. 12 presents the predicted combustion efficiency and gross indicated thermal efficiency (ITE) for all simulation cases. At this low-load operating point, all cases exhibit relatively low combustion efficiency, with the RCCI cases performing worse than the CDF baseline. This reduction is attributed to incomplete methanol oxidation in the near-wall regions of the cylinder liner, as illustrated in Fig. 11. Among the RCCI points, RCCI-1 shows the lowest combustion efficiency due to its ultra-lean condition ($\lambda = 7.4$), resulting in the highest THC emissions, as shown in Fig. 13. Across all simulation cases, combustion efficiency and THC emissions are inversely proportional to the air-excess ratio (λ). Specifically, leaner methanol–air mixtures promote flame quenching near the walls, lowering combustion efficiency and increasing THC. With respect to gross ITE, the RCCI-2 case exhibits an improvement over the CDF simulation due to its faster combustion and lower combustion temperature, which reduce wall heat losses. Finally, the CO emissions are higher in the CDF baseline as the late heptane injection produces locally rich, diffusion-controlled reaction zones. These zones react without

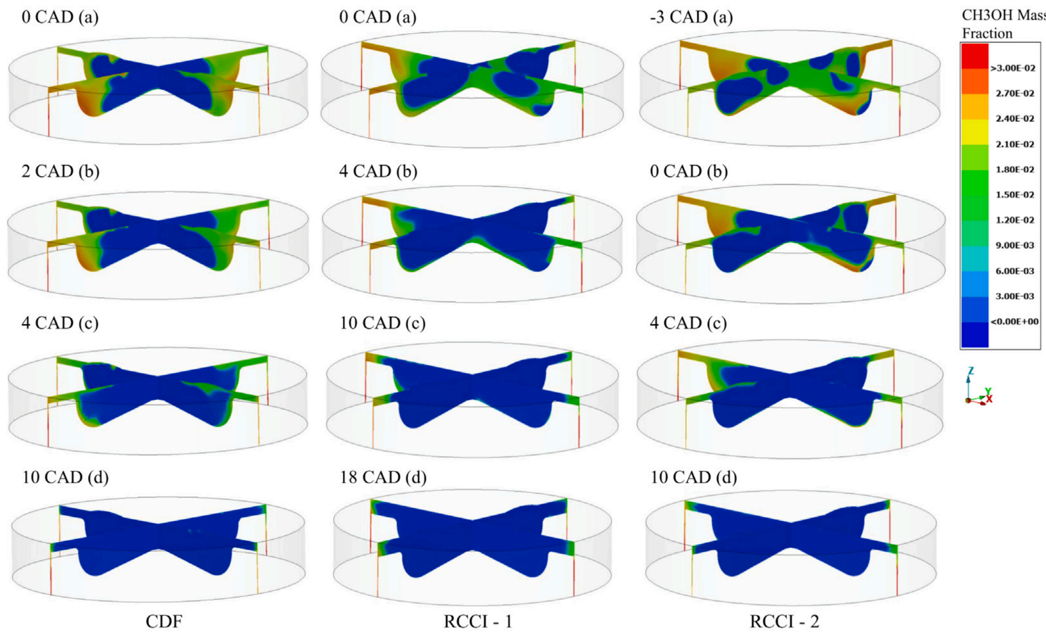

(a) Consumption of methanol during flame propagation

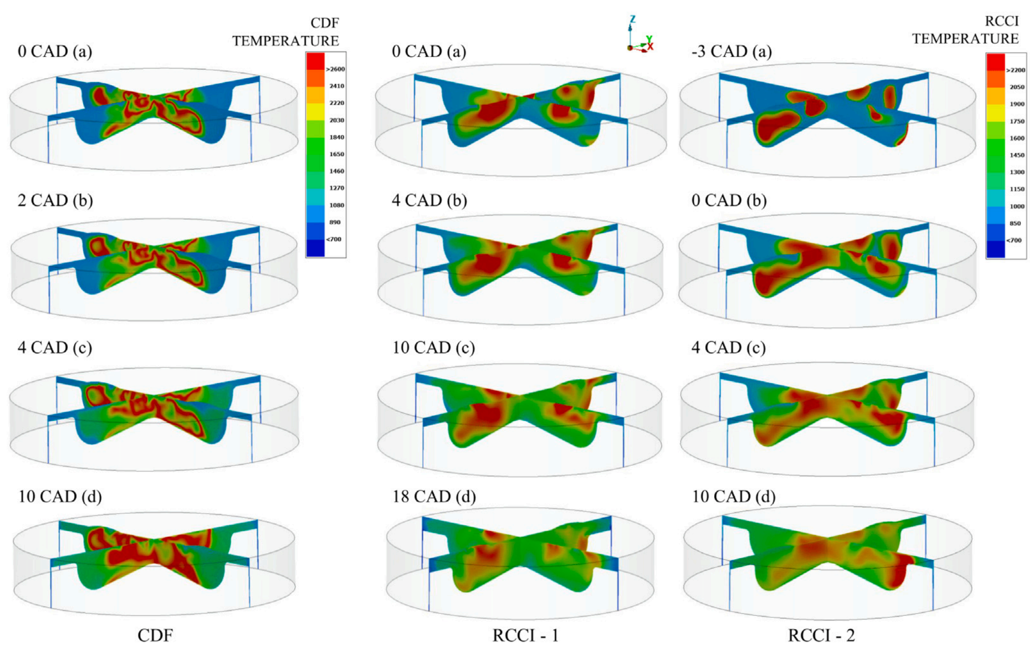

(b) Temperature contours during flame propagation

Fig. 10. Methanol mass fractions and temperature contours during flame propagation. Each row of snapshots corresponds approximately to CA25, CA50, CA90 and end of combustion for each operating condition.

sufficient oxygen for complete oxidation, allowing CO formation during high-temperature reactions.

The RCCI-2 case already uses a high BR in 64%. An increase of BR causes combustion efficiency to drop. Whereas such BR variation is not presented in this study, we have already shown the same behaviour for the CDF case in Bùi et al. [55]. To improve combustion efficiency, we propose modifications to the injection system, such as using higher diesel injection pressures or diesel multipulse injection strategies to enhance atomisation and promote a more uniform HRF distribution. Another approach could be to advance the diesel start of injection and investigate whether additional premixing could increase reactivity and mitigate methanol's inhibitory effect. Lastly, increasing the intake air temperature could mitigate methanol partial burning; however, this measure must be applied with caution, as excessive increases may lead to engine knocking.

In Fig. 13, the NOx model predictions show adequate agreement with the respective experimental measurements. The lower overall combustion temperatures in the RCCI cases lead to a significant decrease in NOx emissions, by up to a factor of four compared to the CDF baseline. Across all simulations, the total in-cylinder NOx is slightly higher than the measured exhaust values. Fig. 14 shows the NOx mass contours (in kg) using similar cut-planes as in Section 4.2.3. We set an increased

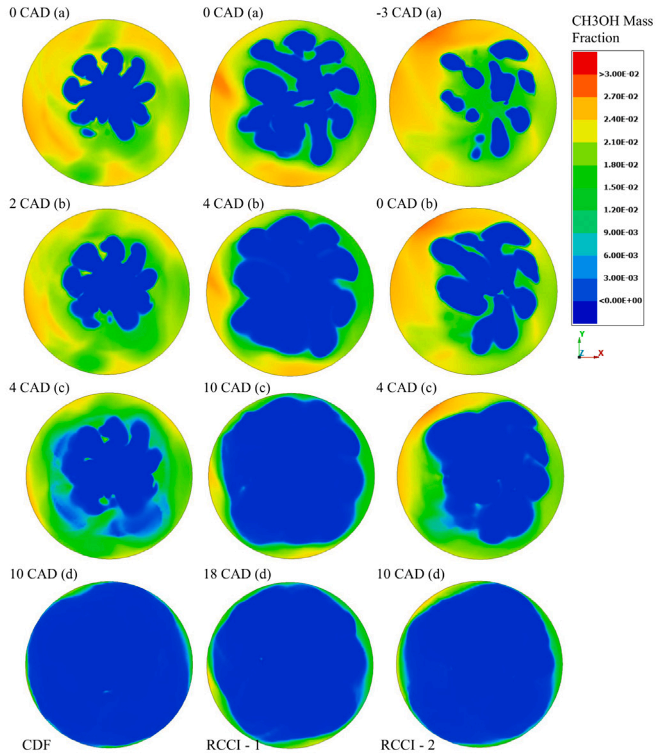

(a) Consumption of methanol during flame propagation

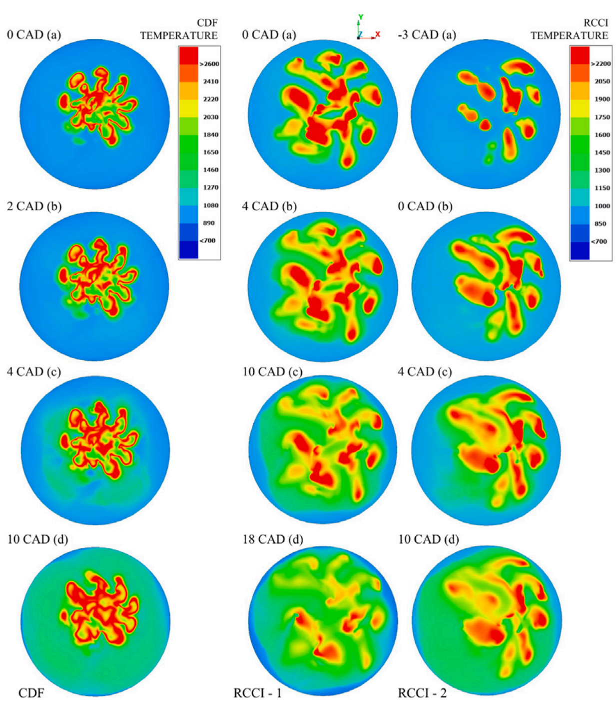

(b) Temperature contours during flame propagation

Fig. 11. Methanol mass fractions and temperature contours at z = −1.5 mm XY-plane during flame propagation. Each row of snapshots corresponds approximately to CA25, CA50, CA90 and end of combustion for each operating condition.

contour threshold for the CDF case due to its substantially elevated NOx concentrations. The NOx contours are shown at later crank angles than the fuel and temperature ignition contours as NOx formation is

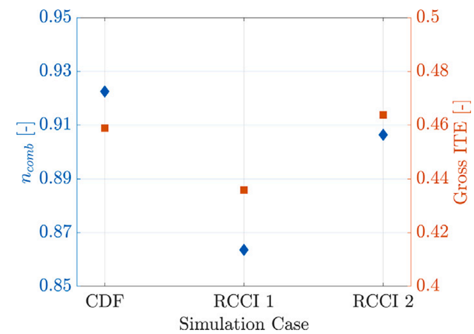

Fig. 12. Combustion efficiency and gross indicated thermal efficiency for the simulated cases.

cumulative and mainly develops after the formation of high-temperature reaction zones. Therefore, the selected NOx snapshots correspond to the late combustion period, when differences in accumulated NOx mass are more visible. These contours highlight the NOx formation regions, which align with the high-temperature regions presented in Fig. 11(b). As illustrated in the figure, the main NOx formation spots are located within the hot heptane reaction zones around the spray plumes in the CDF case and in the vicinity of the heptane ignition kernel locations in the RCCI cases. Ultimately, our observations demonstrate that NOx is mainly produced during the high-temperature heptane combustion phase. In the RCCI cases, diesel premixing reduces these temperatures, while methanol contributes only marginally to the overall NOx formation.

5. Conclusions

In this work, we developed a three-dimensional CFD model of a methanol–diesel single-cylinder marine engine. Using the model, we simulated methanol reactivity-controlled compression ignition (RCCI) operation at a low load condition of 3.1 bar BMEP, using the SAGE detailed chemistry solver combined with our previously validated spray framework. The simulations reproduced in-cylinder pressure and AHRR for both a conventional dual-fuel (CDF) baseline combustion mode and two RCCI operating points, accurately capturing ignition timing and the overall combustion trends. Compared to CDF, RCCI exhibited smoother, more spatially distributed heat release and reduced peak temperatures, resulting in comparable or improved gross ITE and significantly lower NOx emissions. Using the CFD model insights, we linked these outcomes to earlier diesel injection and in-cylinder methanol-air reactivity stratification. The former induced heptane-air premixing, reducing the overall temperature of autoignition reactions, while the latter determined the formation of the ignition kernel and the subsequent rapid flame development.

Under very lean methanol conditions, the model showed near-wall flame quenching and incomplete oxidation, resulting in elevated THC emissions and reduced combustion efficiency. In addition, we reviewed the hypothesis of the ideal homogeneous mixture scenario, which is a widely adopted practice in methanol-diesel engine simulations. We demonstrated that neglecting mixture stratification, obtained by mixing simulations and the intake stroke, leads to noticeable differences in combustion modelling. Specifically, removing stratification weakened autoignition intensity, slowed methanol consumption and lowered peak cylinder pressure. These findings indicate that RCCI performance depends on spatial reactivity stratification, in which the diesel-rich areas initiate reactions in methanol-lean pockets.

Future work could focus on shaping reactivity stratification through fuel-air mixing studies. This could be realised by comparing various piston and intake port designs that affect cylinder swirl and tumble flow, and their potential to achieve favourable conditions for ignition. Moreover, follow-up studies could investigate diesel injection

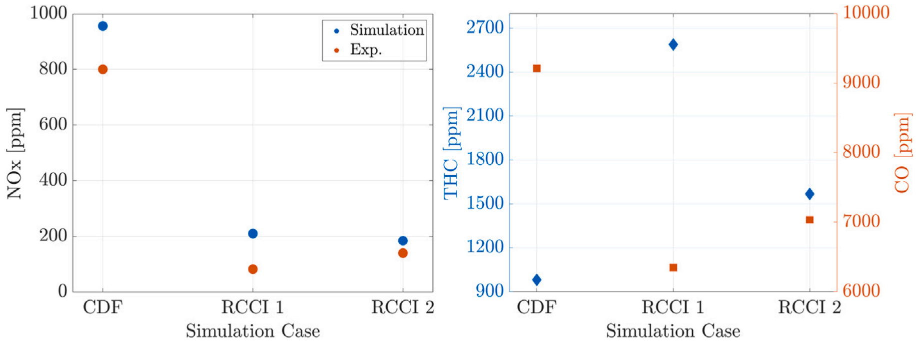

Fig. 13. Concentration of major emission species for the simulated cases.

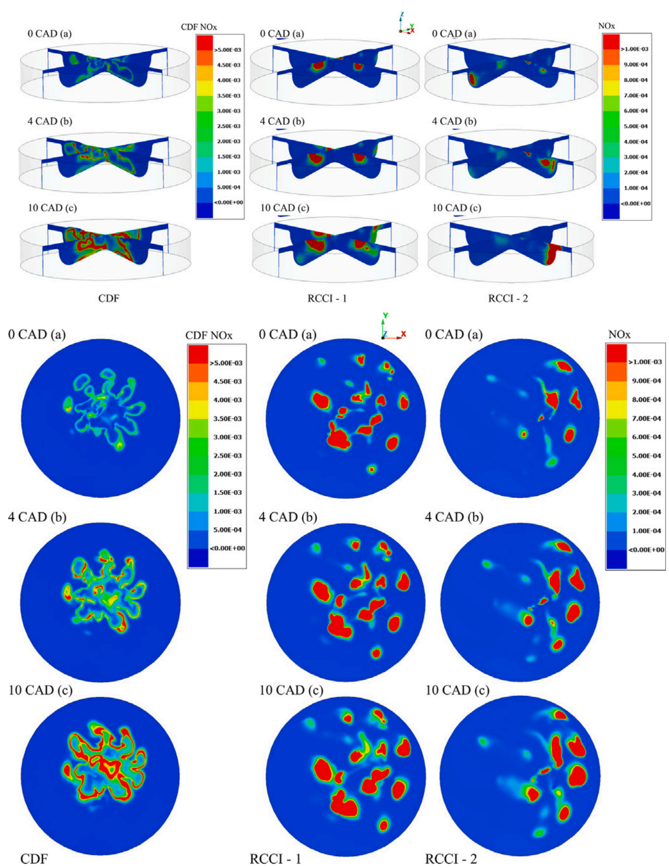

Fig. 14. NOx mass contours during the later stages of combustion. Note that CDF and RCCI have their individual contour legends.

pressure, intake air temperature, diesel multipulse injection strategies, spray-plume cone angle, and the start of injection as means of manipulating the topology of the ignition kernels. Since RCCI ignition is a combined effect of low methanol and high diesel concentrations, additional high-fidelity CFD studies (e.g., Large Eddy Simulation or Direct Numerical Simulation of ignition) could reveal the ignition phenomena associated with methanol's reaction-inhibition effects. Additionally, modelling studies should extend the RCCI validation across load points, enabling generalisation of the present conclusions to higher in-cylinder temperatures and different air-excess ratios. This will increase the credibility of CFD modelling in robustly capturing engine-related phenomena. Our study offers valuable insights into the modelling of methanol RCCI engines, potentially advancing sustainable methanol-powered marine engines.

CRediT authorship contribution statement

Konstantinos Zoumpourlos: Writing – original draft, Visualization, Validation, Software, Methodology, Investigation, Formal analysis, Data curation, Conceptualization. **Cemil Bekdemir:** Writing – review & editing, Methodology, Formal analysis, Conceptualization. **Konstantinos Ioannis Kiouranakis:** Writing – review & editing, Investigation, Formal analysis. **Rinze Geertsma:** Writing – review & editing, Supervision, Resources, Project administration, Formal analysis. **Robert van de Ketterij:** Writing – review & editing, Supervision, Project administration, Funding acquisition. **Andrea Coraddu:** Writing – review & editing, Supervision, Project administration, Funding acquisition.

Declaration of competing interest

The authors declare that they have no known competing financial interests or personal relationships that could have appeared to influence the work reported in this paper.

Acknowledgements

The present research is part of the MENENS project (Methanol als Energiestap Naar Emissieloze Nederlandse Scheepvaart). The project is funded by the Netherlands Enterprise Agency (RVO: Rijksdienst voor Ondernemend Nederland) under the grant number MOB21012.

We would like to thank Convergent Science [57], and BETA CAE Systems [76] for offering their software (CONVERGE, ANSA and META) and their technical support for the accomplishment of this research. ANSA was used for the geometry manipulation and pre-processing of the CFD model, CONVERGE for the CFD simulations, and META for post-processing and visualisation of the results. This work used the Dutch national e-infrastructure with the support of the SURF Cooperative using grant no. EINF-12527. Additionally, part of the simulations were run on the DelftBlue supercomputer [77].

Data availability

The data that has been used is confidential.

References

[1] Reitz RD, Ogawa H, Payri R, Fansler T, Kokjohn S, Moriyoshi Y, Agarwal A, Arcoumanis D, Assanis D, Bae C, Boulouchos K, Canakci M, Curran S, Denbratt I, Gavaises M, Guenthner M, Hasse C, Huang Z, Ishiyama T, Johansson B, Johnson T, Kalghatgi G, Koike M, Kong S, Leipertz A, Miles P, Novella R, Onorati A, Richter M, Shuai S, Siebers D, Su W, Trujillo M, Uchida N, Vaglieco BM, Wagner R, Zhao H. IJER editorial: the future of the internal combustion engine. Int J Engine Res 2020. https://doi.org/10.1177/1468087419877990

[2] Curran S, Onorati A, Payri R, Agarwal AK, Arcoumanis C, Bae C, Boulouchos K, Dal Forno Chuahy F, Gavaises M, Hampson GJ, et al. The future of ship engines: renewable fuels and enabling technologies for decarbonization; 2023.

[3] International Maritime Organization. International maritime organization: fourth greenhouse gas study 2020, Technical Report, 2020 https://www.imo.org/en/OurWork/Environment/Pages/Fourth-IMO-Greenhouse-Gas-Study-2020.aspx [Accessed: 5 February 2023].

[4] Kessel DG. Global warming—facts, assessment, countermeasures. J Pet Sci Eng 2000;26:157–68.
[5] Nemati A, Ong JC, Walther JH. CFD analysis of combustion and emission formation using URANS and LES under large two-stroke marine engine-like conditions. Appl Therm Eng 2022;216:119037.
[6] Verhelst S, Turner JW, Sileghem L, Vancoillie J. Methanol as a fuel for internal combustion engines. Prog Energy Combust Sci 2019;70.
[7] Svanberg M, Ellis J, Lundgren J, Landälv I. Renewable methanol as a fuel for the shipping industry. Renew Sustain Energy Rev 2018. https://doi.org/10.1016/j.rser.2018.06.058
[8] Zincir B, Deniz C. Methanol as a fuel for marine diesel engines. In: Energy, environment, and sustainability. Springer Nature; 2021. p. 45–85. https://doi.org/10.1007/978-981-16-0931-2_4
[9] Pipicelli M, Di Luca G, Ianniello R, Gimelli A, Beatrice C. Alcohol fuels in compression ignition engines. In: Energy, environment, and sustainability. Springer Nature; 2022. p. 9–31. https://doi.org/10.1007/978-981-16-8751-8_2
[10] Flynn P, Hunter G, Farrel L, Durrett R, Akinyemi O, Zur Loye A, Westbrook C, Pitz W. The inevitability of engine-out NOx emissions from spark-ignited and diesel engines. Proc Combust Inst 2000. https://doi.org/10.1016/S0082-0784(00)80332-X
[11] Ryan TW, Maymar M, Ott D, LaViolette RA, MacDowall RD. Combustion and emissions characteristics of minimally processed methanol in a diesel engine without ignition assist. In: SAE technical paper; 1994. https://doi.org/10.4271/940326
[12] Mahendar SK, Erlandsson A, Adlercreutz L. Challenges for spark ignition engines in heavy duty application: a review. In: SAE technical paper series; 2018. https://doi.org/10.4271/2018-01-0907
[13] Karim GA. Dual-fuel diesel engines. CRC Press; 2015. https://doi.org/10.1201/b18163
[14] Repo J, Axelsson M, Heir V. Methanol combustion concept alternatives for new build and retrofit of 4-stroke medium speed engines. In: 30th CIMAC world congress. Busan, Korea; 2023.
[15] Kiouranakis KI, Vos PD, Geertsma R. Methanol as a fuel in shipping: review and outlook to ICE research within MENENS. In: Transport transitions: advancing sustainable and inclusive mobility; 2025. https://doi.org/10.1007/978-3-031-89444-2_106
[16] Kiouranakis KI, de Vos P, Zoumpourlos K, Coraddu A, Geertsma R. Methanol for heavy-duty internal combustion engines: review of experimental studies and combustion strategies. Renew Sustain Energy Rev 2025;214.
[17] Attard WP, Toulson E, Huisjen A, Chen X, Zhu G, Schock H. Spark ignition and pre-chamber turbulent jet ignition combustion visualization. In: SAE technical paper; 2012. https://doi.org/10.4271/2012-01-0823
[18] Kiouranakis KI, Vos PD, Willems R, Sapra HD, Geertsma R. Heat release behavior in a natural gas lean-burn SI marine engine: exploring the impact of bowl-in and squish combustion on performance and emissions. Appl Therm Eng 2025. https://doi.org/10.1016/j.applthermaleng.2025.127509
[19] Splitter D, Szybist J, Jatana G, Svensson K, Montgomery D. Approach for high methanol substitution by energy with conventional and bio pilot fuels. In: 31st CIMAC world congress. Zurich; 2025.
[20] Stenzel K, Thorau P, Beckmann L, Schirrmeister F, Reiser C, Buchholz B. Experimental investigations of a methanol dual-fuel combustion process for marine engines. In: 31st CIMAC world congress. Zurich; 2025.
[21] Wang Q, Wei L, Pan W, Yao C. Investigation of operating range in a methanol fumigated diesel engine. Fuel 2015;140:164–70. https://doi.org/10.1016/j.fuel.2014.09.067
[22] Dierickx J, Verbiest J, Janvier T, Peeters J, Sileghem L, Verhelst S. Retrofitting a high-speed marine engine to dual-fuel methanol-diesel operation: a comparison of multiple and single point methanol port injection. Fuel Commun 2021;7:10.
[23] Noguchi M, Tanaka Y, Tanaka T, Takeuchi Y. A study on gasoline engine combustion by observation of intermediate reactive products during combustion. In: SAE technical paper. Milwaukee, Wisconsin, United States; 1979. https://doi.org/10.4271/790840
[24] Chen Z, Konno M, Oguma M, Yanai T. Experimental study of CI Natural-Gas/DME homogeneous charge engine. In: SAE 2000 world congress; 2000. https://doi.org/10.4271/2000-01-0329
[25] Furutani M, Isogai T, Ohta Y. Ignition characteristics of gaseous fuels and their difference elimination for SI and HCCI gas engines. In: Combustion, explosion, and shock waves; 2003. https://doi.org/10.4271/2003-01-1857
[26] Zheng Z, Yao M, Chen Z, Zhang B. Experimental study on HCCI combustion of dimethyl ether(DME)/Methanol dual fuel. In: 2004 powertrain & fluid systems conference & exhibition; 2004. https://doi.org/10.4271/2004-01-2993
[27] Shudo T, Takahashi T. Influence of reformed gas composition on HCCI combustion of onboard methanol-reformed gases. In: 2004 SAE fuels & lubricants meeting & exhibition; 2004. https://doi.org/10.4271/2004-01-1908
[28] Kokjohn SL, Hanson RM, Splitter DA, Reitz RD. Experiments and modeling of dual-fuel HCCI and PCCI combustion using in-cylinder fuel blending. SAE Int J Engines 2009. https://doi.org/10.4271/2009-01-2647
[29] Persson H, Hultqvist A, Johansson B, Remón A. Investigation of the early flame development in spark assisted HCCI combustion using high speed chemiluminescence imaging. In: SAE 2011 world congress & exhibition; 2007. https://doi.org/10.4271/2007-01-0212
[30] Yao M, Zheng Z, Liu H. Progress and recent trends in homogeneous charge compression ignition (HCCI) engines. Prog Energy Combust Sci 2009. https://doi.org/10.1016/j.pecs.2009.05.001
[31] Kokjohn SL, Musculus MP, Reitz RD. Evaluating temperature and fuel stratification for heat-release rate control in a reactivity-controlled compression-ignition engine using optical diagnostics and chemical kinetics modeling. Combust Flame 2015. https://doi.org/10.1016/j.combustflame.2015.04.009
[32] Inagaki K, Fuyuto T, Nishikawa K, Nakakita K, Sakata I. Dual-fuel PCI combustion controlled by in-cylinder stratification of ignitability. In: 2006 SAE world congress; 2006. https://doi.org/10.4271/2006-01-0028
[33] Reitz RD, Duraisamy G. Review of high efficiency and clean reactivity controlled compression ignition (RCCI) combustion in internal combustion engines. Prog Energy Combust Sci 2015. https://doi.org/10.1016/j.pecs.2014.05.003
[34] Bessonette PW, Schleyer CH, Duffy KP, Hardy WL, Liechty MP. Effects of fuel property changes on heavy-duty HCCI combustion. In: SAE world congress & exhibition; 2007. https://doi.org/10.4271/2007-01-0191
[35] Yao C, Cheung C, Cheng C, Wang Y, Chan T, Lee S. Effect of diesel/methanol compound combustion on diesel engine combustion and emissions. Energy Convers Manag 2008;49:1696–704. https://doi.org/10.1016/j.enconman.2007.11.007
[36] Dec JE, Yang Y, Dronniou N. Boosted HCCI - controlling pressure-rise rates for performance improvements using partial fuel stratification with conventional gasoline. SAE Int J Engines 2011. https://doi.org/10.4271/2011-01-0897
[37] Yang Y, Dec JE, Dronniou N, Sjöberg M. Tailoring HCCI heat-release rates with partial fuel stratification: comparison of two-stage and single-stage-ignition fuels. Proc Combust Inst 2011. https://doi.org/10.1016/j.proci.2010.06.114
[38] Dec JE, Yang Y, Dronniou N. Improving efficiency and using E10 for higher loads in boosted HCCI engines. SAE Int J Engines 2012. https://doi.org/10.4271/2012-01-1107
[39] Singh G, Singh AP, Agarwal AK. Experimental investigations of combustion, performance and emission characterization of biodiesel fuelled HCCI engine using external mixture formation technique. Sustain Energy Technol Assess 2014. https://doi.org/10.1016/j.seta.2014.01.002
[40] Lu X, Han D, Huang Z. Fuel design and management for the control of advanced compression-ignition combustion modes. Prog Energy Combust Sci 2011. https://doi.org/10.1016/j.pecs.2011.03.003
[41] Stanglmaier RH, Roberts CE. Homogeneous charge compression ignition (HCCI): benefits, compromises, and future engine applications. In: SAE technical paper series; 1999. https://doi.org/10.4271/1999-01-3682
[42] Yang X, Zhu GG, Sun Z. A control oriented SI and HCCI hybrid combustion model for internal combustion engines. In: ASME; 2010. https://doi.org/10.1115/DSCC2010-4042
[43] Cao Y, Xue Z, Miao Q, Deng J, Li L. Closed loop control of SI/HCCI combustion mode switch based on ion current feedback. In: SAE technical paper; 2014. https://doi.org/10.4271/2014-01-2704
[44] Benajes J, Pastor JV, García A, Monsalve-Serrano J. The potential of RCCI concept to meet EURO VI NOx limitation and ultra-low soot emissions in a heavy-duty engine over the whole engine map. Fuel 2015. https://doi.org/10.1016/j.fuel.2015.07.064
[45] Lu X, Ji L, Zu L, Hou Y, Huang C, Huang Z. Experimental study and chemical analysis of n-heptane homogeneous charge compression ignition combustion with port injection of reaction inhibitors. Combust Flame 2007. https://doi.org/10.1016/j.combustflame.2007.01.002
[46] Xu H, Yao C, Xu G. Chemical kinetic mechanism and a skeletal model for oxidation of n-heptane/methanol fuel blends. Fuel 2012. https://doi.org/10.1016/j.fuel.2011.09.048
[47] Zhu J, Li J, Wang S, Raza M, Qian Y, Feng Y, Yu L, Mao Y, Lu X. Ignition delay time measurements and kinetic modeling of methane/diesel mixtures at elevated pressures. Combust Flame 2021. https://doi.org/10.1016/j.combustflame.2021.02.036
[48] Zou X, Wang H, Zheng Z, Reitz R, Yao M. Numerical study of the RCCI combustion processes fuelled with methanol, ethanol, n-Butanol and diesel. In: SAE 2016 world congress and exhibition; 2016, pp. 2016–01–0777. https://doi.org/10.4271/2016-01-0777
[49] Li Y, Jia M, Xu L, Bai X-S. Multiple-objective optimization of methanol/diesel dual-fuel engine at low loads: a comparison of reactivity controlled compression ignition (RCCI) and direct dual fuel stratification (DDFS) strategies. Fuel 2020;262:116673.
[50] Zhou DZ, Yang WM, An H, Li J. Application of CFD-chemical kinetics approach in detecting RCCI engine knocking fuelled with biodiesel/methanol. Appl Energy 2015;145:255–64. https://doi.org/10.1016/j.apenergy.2015.02.058
[51] Li Y, Jia M, Liu Y, Xie M. Numerical study on the combustion and emission characteristics of a methanol/diesel reactivity controlled compression ignition (RCCI) engine. Appl Energy 2013;106:184–97. https://doi.org/10.1016/j.apenergy.2013.01.058
[52] Zoumpourlos K, Geertsma R, Van De Ketterij R, Coraddu A. Methanol operation in heavy-duty DICI dual-fuel engines: investigating charge cooling effects using ECN spray D data. J Eng Gas Turbines Power 2025;1–10. https://doi.org/10.1115/1.4067862
[53] Zoumpourlos K, Bekdemir C, Geertsma R, van de Ketterij R, Coraddu A. CFD modeling approach for late-injection methanol sprays validated with ECN spray M. Int J Engine Res 2025;14680874251323931.
[54] Zoumpourlos K, Bekdemir C, Geertsma R, van de Ketterij R, Coraddu A. Methanol sprays in marine engines: CFD modelling of port fuel injection systems. J Mar Eng Technol 2025;1–17.
[55] Bùi G, Zoumpourlos K, Bekdemir C, Somers B. Numerical investigation of methanol-air mixture formation and combustion in a dual-fuel marine engine at low load. Fuel 2026;413:138208.
[56] Kiouranakis KI, Willems R, de Vos P, Geertsma R. Combustion mode analysis of a large-bore methanol premixed dual-fuel engine with high methanol energy fractions. Energy Convers Manag X 2025;101417.
[57] CONVERGE CFD software website. 2023. https://convergecfd.com/.
[58] Convergent Science Inc. Converge manual v3.0. 2022.
[59] Senecal P, Pomraning E, Richards K, Som S. Grid-convergent spray models for internal combustion engine CFD simulations. In: Internal combustion engine division fall technical conference, 55096. American Society of Mechanical Engineers; 2012. p. 697–710.

[60] Karvounis P, Theotokatos G, Zoumpourlos K, Coraddu A. Parametric optimisation of methanol combustion in marine dual-fuel engines at low loads. Appl Therm Eng 2025;128652.
[61] Wei F, Zhang Z, Wei W, Zhang H, Cai W, Dong D, Li G. Multi-objective optimization of the performance for a marine methanol-diesel dual-fuel engine. Fuel 2024;368:131556.
[62] Karvounis P, Theotokatos G, Patil C, Xiang L, Ding Y. Parametric investigation of diesel–methanol dual fuel marine engines with port and direct injection. Fuel 2025;381:133441.
[63] Han Z, Reitz RD. Turbulence modeling of internal combustion engines using RNG κ-ε models. Combust Sci Technol 1995;106:267–95.
[64] Richards KJ, Senecal PK, Pomraning E. CONVERGE 3.0. Convergent Science, Madison, WI 540. 2021.
[65] Reitz RD, Diwakar R. Structure of high-pressure fuel sprays. SAE Trans 1987;492–509.
[66] Beale JC, Reitz RD. Modeling spray atomization with the Kelvin-Helmholtz/Rayleigh-Taylor hybrid model. At Sprays 1999;9.
[67] Schmidt DP, Rutland CJ. A new droplet collision algorithm. J Comput Phys 2000;164:62–80.
[68] Post SL, Abraham J. Modeling the outcome of drop–drop collisions in diesel sprays. Int J Multiph Flow 2002;28:997–1019.
[69] Kuhnke D. Spray/wall-interaction modelling by dimensionless data analysis; 2004.
[70] Liu S, Sun T, Zhou L, Jia M, Zhao W, Wei H. A new skeletal kinetic model for methanol/n-heptane dual fuels under engine-like conditions. Energy 2023;263:125648.
[71] Curran HJ, Gaffuri P, Pitz WJ, Westbrook CK. A comprehensive modeling study of n-heptane oxidation. Combust Flame 1998;114:149–77.
[72] Pomraning E, Richards K, Senecal P. Modeling turbulent combustion using a RANS model, detailed chemistry, and adaptive mesh refinement. Technical Report SAE Technical Paper; 2014.
[73] Kokjohn SL, Hanson RM, Splitter D, Reitz R. Fuel reactivity controlled compression ignition (RCCI): a pathway to controlled high-efficiency clean combustion. Int J Engine Res 2011;12:209–26.
[74] Reitz RD, Duraisamy G. Review of high efficiency and clean reactivity controlled compression ignition (RCCI) combustion in internal combustion engines. Prog Energy Combust Sci 2015;46:12–71.
[75] Karimkashi S, Gadalla M, Kannan J, Tekgül B, Kaario O, Vuorinen V. Large-eddy simulation of diesel pilot spray ignition in lean methane-air and methanol-air mixtures at different ambient temperatures. Int J Engine Res 2023;24:965–81.
[76] BETA CAE systems website. 2023. https://www.beta-cae.com/.
[77] Delft High Performance Computing Centre (DHPC). DelftBlue supercomputer (Phase 1); 2022. https://www.tudelft.nl/dhpc/ark/delftbluephase1.